FLUID SIMULATIONS OF ∇T_e-DRIVEN TURBULENCE AND TRANSPORT IN BOUNDARY PLASMAS

by

X. Q. Xu

FLUID SIMULATIONS OF ∇T_e-DRIVEN TURBULENCE AND TRANSPORT IN BOUNDARY PLASMAS

by

X. Q. Xu

Memorandum No. UCB/ERL M92/147

15 December 1992

ELECTRONICS RESEARCH LABORATORY

College of Engineering
University of California, Berkeley
94720

FLUID SIMULATIONS OF ∇T_e-DRIVEN TURBULENCE AND TRANSPORT IN BOUNDARY PLASMAS

by

X. Q. Xu

ELECTRONICS RESEARCH LABORATORY

College of Engineering
University of California, Berkeley
94720

Fluid Simulations of ∇T_e-Driven Turbulence and Transport in Boundary Plasmas

X.Q. Xu

Electronics Research Laboratory

University of California, Berkeley, California 94720

Abstract

It is clear that the edge plasma plays a crucial role in global tokamak confinement. This paper is a report on simulations of a new drift wave type instability driven by the electron temperature gradient (∇T_e, ETG) in tokamak scrapeoff-layers (SOL)[1]. A $2d(x,y)$ fluid code has been developed in order to explore the anomalous transport in the boundary plasmas. The simulation consists of a set of fluid equations (in the electrostatic limit) for the vorticity $\nabla_\perp^2 \phi$, the electron density n_e and the temperature T_e in a shearless plasma slab confined by a uniform, straight magnetic field B_z with two divertor (or limiter) plates intercepting the magnetic field. The model has two regions separated by a magnetic separatrix: in the edge region inside the separatrix, the model is periodic along the magnetic field while in the SOL region outside the separatrix, the

magnetic field is taken to be of finite length with model (logical sheath) boundary conditions at diverter (or limiter) plates. The simulation results show that the observed linear instability agrees well with theory, and that a saturated state of turbulence is reached. In saturated turbulence, clear evidence of the expected long-wavelength mode penetration into the edge is seen, an inverse cascade of wave energy (toward both long wavelengths and low frequencies) is observed. The simulation results also show that amplitudes of potential and the electron temperature fluctuations are somewhat above and the heat flux are somewhat below those of the simplest mixing-length estimates, and furthermore the large-scale radial structures of fluctuation quantites indicate that the cross-field transport is not diffusive. After saturation, the electron density and temperature profiles are flattened. A self-consistent simulation to determine the microturbulent SOL electron temperature profile has been done, the results of which reasonably agree with the experimental measurements.

1 Introduction

This paper presents turbulence simulations in the tokamak boundary plasmas. The tokamak boundary plasma is defined here as the scrape-off layer (SOL) through the last closed flux surface (LCFS) near the magnetic separatrix, and thus includes both open and closed field lines. The SOL plasma is distinguished from the edge plasma by the presence of

2

magnetic field lines connected to the divertor (or limiter) plates. The dynamics of tokamak boundary plasmas have proven to be critical in determining the overall confinement of the plasma discharge([2],[3],[4],[5]). A striking characteristic of a boundary plasma is that it is extremely turbulent, with observed fluctuation levels of up to 50% (as opposed to only a few percent in the core plasma). The implication of the boundary turbulence is twofold. First, the determination of a microturbulent SOL width and the power-handling capability of a divertor (or limiter) is considered to be a major issue for the design of future large tokamaks such as ITER. A high level of the SOL turbulence is desirable, since high peak power and high electron temperature at the endplate are to be avoided (which otherwise result in substantial problems associated with sputtering). Second, divertor (or limiter) configurations play a very important role in determining the cause of the negative electric field E_r shear layer([6], [7], [8], [9]), which is believed to cause a reduced edge plasma fluctuation levels, and improved confinement of the main plasma discharge ([2],[3],[4]).

The SOL is the portion of a tokamak plasma located in the open-field line region, bounded on one side by the last closed magnetic flux surface with hot edge plasma, and on the other side by the inner wall of the vacuum vessel. Several instabilities in the SOL have been analyzed and the electron-temperature-gradient (ETG, ∇T_e) driven instability has been identified as the most dominant known mode[10]. This instability, with drift-

wave characteristics, is driven by an electron temperature gradient in the presence of the Kunkel-Guillory sheath impedance[11]. The linear analysis of this conducting-wall-induced instability shows that it has robust growth rate for parameters relevant to the tokamak boundary plasmas. The maximum growth rate occurs for $k_y \rho_s \simeq 0.1$ for typical DIII-D parameters. At long-wavelengths, electron energy end-losses stabilize the ETG-mode, while at short-wavelengths the cut-off is due to finite-Larmor-radius (FLR) effects as well as classical diffusion and viscosity. Although the predicted instability has characteristics similar to experimental edge fluctuation data, the mixing-length estimated transport exceeds the experimental value. Hence a basic understanding of the mechanism for the nonlinear saturation of the ETG-mode and the determination of its penetration inside the separatrix is desirable.

The understanding of the handling of the power carried by the charged particles (electrons and ions) into the scrapeoff layer of the tokamak is a central issue in the boundary plasmas and remains a major obstacle for the proposed ITER tokamak for its continuous and reliable operation. The nominal analysis of the SOL assumes that the power entering the SOL is equal to that crossing the separatrix. The power crossing the separatrix into the SOL is transported radially as well as axially (i. e., along the magnetic field lines); the power transported axially in the SOL is lost at the endplates. Depending

on the the SOL plasma collisionality regime, the axial transport of power is either in the gradient-limited regime (collisional) or the flux-limited regime (less collisional). When the electron-conduction power is flux-limited, it has been shown[12] that the electron and ion temperatures are decoupled, and the SOL is separated into two radial scale-lengths: a short scale associated with the electron-conduction layer ($\sim$ 1cm); and a longer radial scale associated with an energy-exchange layer ($\sim$3cm) in which the ion power is collisionally transfered to a cold electron plasma. The experimental evidence indicates that the radial transport is anomalously large. The mechanism behind the SOL turbulence remains unclear. The anomalous radial transport competing with the axial classical flow sets the SOL electron temperature and density profiles. With this conjecture in mind, we develop a self-consistent simulation code to explore the SOL electron temperature profile in the electron-conduction layer based on the ETG driven turbulence.

This paper describes some features of the nonlinear saturation of the ETG-mode and the SOL electron temperature profile due to the turbulence. In Section II, a model sheath physics and the basic geometry for the 2d simulations are presented. The 2d nonlinear equations for a boundary plasma are given in Section III. A review of linear theories with an extension including the energy end-losses and a brief review of the numerical scheme will also be presented. Section IV discusses nonlinear results from the 2d simulations.

Section V explores the SOL electron temperature profile with power crossing the separatrix.
Summaries and conclusions are presented in Section VI.

2 Basic model and Model Sheath Physics

To characterize the region of boundary plasmas across the magnetic separatrix of a tokamak with a limiter (or divertor), a simple slab model is chosen which includes the two regions identified in Fig. 1: the plasma (in a shearless magnetic field $\mathbf{B}(x) = B_0 \mathbf{e_z}$) is periodic along the axial (z) direction in the edge ($x < x_{sp}$) and is confined at the ends by two conducting plates in the SOL outside the magnetic separatrix ($x > x_{sp}$). The equilibrium quantities such as $T_i(x), T_e(x)$, and $n_e(x)$ are taken to vary transversely to magnetic field lines in the x-direction.

The SOL can be divided into two markedly different regions: (1) a narrow sheath region (sheath + presheath) ahead of the plate with large equilibrium gradients along the z-direction (on the order of the Debye length); and (2) in contrast to the sheath, a large bulk region away from the sheath region with relatively weak equilibrium gradients. The sheath, due to its small spatial scale, hence is treated here as a boundary condition (see Eq. (1) below). In the SOL region outside the separatrix, the fluid quantities should satisfy the sheath current and the energy flux boundary condition at the sheath edge. The expression
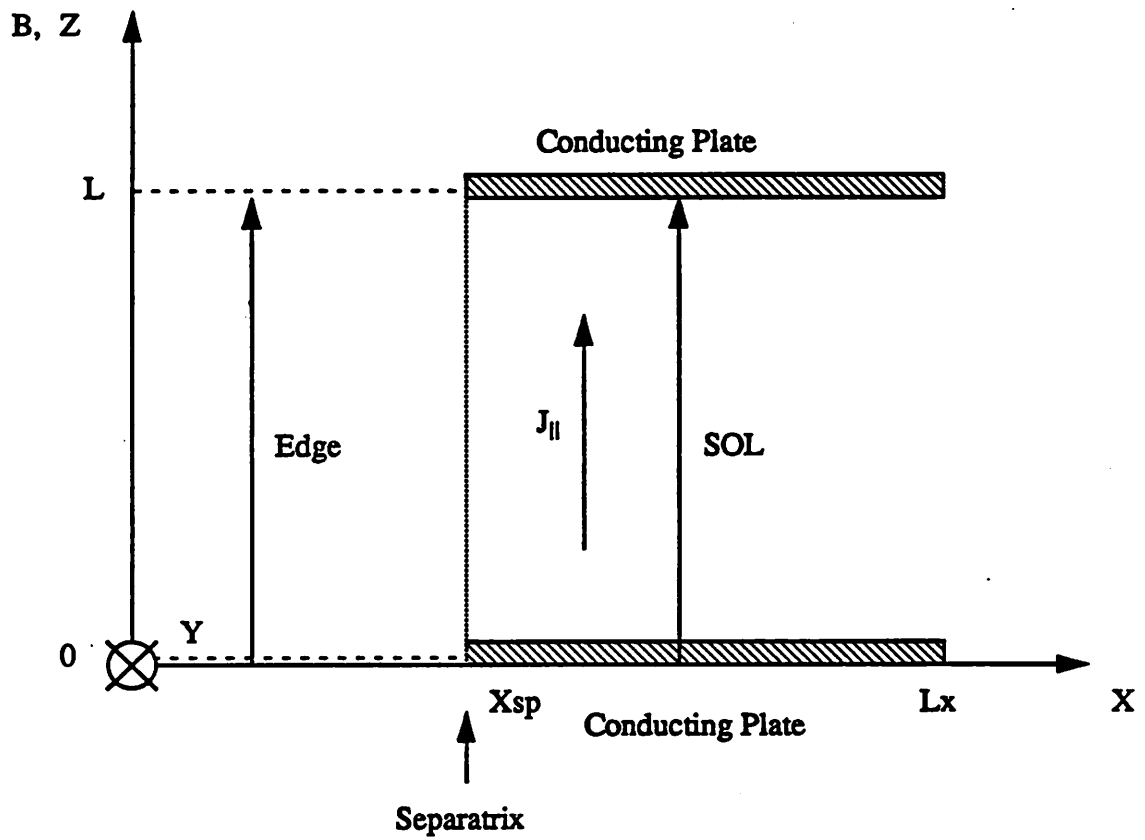
6

Figure 1:   2d slab model for fluid simulations extending across a magnetic separatrix.

for the plasma current near the sheath is

$$j_\parallel^w(L) = -j_\parallel^w(0) = n_s e c_s \left[1 - \frac{v_{T_e}}{2 c_s \sqrt{\pi}} e^{-\frac{e\Phi}{T_e}} \right] \tag{1}$$

where $c_s = \sqrt{\frac{T_i + T_e}{m_i}}$ is the sound speed, $v_{T_e} = \sqrt{\frac{2 T_e}{m_e}}$ the electron thermal velocity. The mass difference between electrons and ions results in a large space-charge potential, and an ambipolar flow to the wall in turn demands equal fluxes of negative and positive charges to the wall. Thus, in equilibrium $J_\parallel^w(0) = J_\parallel^w(L) = 0$, which yields an expression for the amplitude of the equilibrium potential Φ_0:

$$\Lambda \equiv \frac{e\Phi_0}{T_e} = \frac{1}{2} \ln \left[\frac{m_i}{m_e} \frac{2 T_e}{T_i + T_e} \frac{K_i^2}{4\pi} \right] , \tag{2}$$

where constant K_i depends on the details of the pre-sheath model with a typical value $K_i \simeq 2$. For typical SOL parameters, $\Lambda \simeq 3 - 4$. The perturbed current $\tilde{j}_\parallel$ is

$$\tilde{j}_\parallel^w(L) = -\tilde{j}_\parallel^w(0) = n_e e c_s \left[\frac{e\tilde{\phi}}{T_e} - \Lambda \frac{\tilde{T}_e}{T_e} \right] , \tag{3}$$

where a finite and constant ion temperature is assumed.

The electric potential at the endplates regulates the end-loss energy flux to the value

$$q_{el} = \frac{n v_{T_e}}{2 \sqrt{\pi}} (2 T_e + e\Phi) \exp(-\frac{e\Phi}{T_e}). \tag{4}$$

which physically means that each exiting electron leaves at the sound speed, $c_s \simeq \frac{v_{T_e}}{2\sqrt{\pi}} \exp(-\frac{e\Phi}{T_e})$ carrying with it a potential energy $e\phi$, and parallel and perpendicular kinetic energy $2 T_e$.

The perturbed energy flux is

$$\tilde{q}_{el} = c_s[(\Lambda^2 + \frac{5}{2}\Lambda + 3)\tilde{T}_e - (\Lambda + 1)e\tilde{\phi}] \tag{5}$$

Eqs. (1) and (4) (or (3) and (5)) will be used as the axial boundary conditions in the SOL region outside the separatrix.

3   Model Equations, Linear Analysis and 2d Fluid Code

The nonlinear evolution for the turbulence in the electrostatic and flute-mode limits is described by the normalized two-dimensional two-field model:

$$\frac{\partial}{\partial t}\nabla_\perp^2\phi - \nabla \cdot \left[\nabla_\perp^2\phi\nabla_\perp\phi \times z\right] = \delta\frac{\partial}{\partial y}\nabla_\perp^2\phi + \mu\nabla_\perp^4\phi + \begin{cases} (\phi - T_e) & x > x_{sp} \\ \\ 0 & x < x_{sp}, \end{cases}$$

$$\frac{\partial}{\partial t}T_e - \nabla \cdot [T_e\nabla_\perp\phi \times z] = -\frac{\partial\phi}{\partial y} + \kappa\nabla_\perp^2 T_e + \begin{cases} (C_\phi\phi - C_T T_e) & x > x_{sp} \\ \\ 0 & x < x_{sp}, \end{cases} \tag{6}$$

where

$$C_T = \nu^{\frac{2}{3}}(\Lambda^2 + \frac{5}{2}\Lambda + 3),$$

$$C_\phi = \nu^{\frac{2}{3}}(\Lambda^2 + \Lambda),$$

Equations (6) are expressed in dimensionless units defined by $\frac{t}{\tau_0} \longrightarrow t$, $\frac{x}{L_0} \longrightarrow x$, $\frac{y}{L_0} \longrightarrow y$,

$$\frac{\tilde{n}_e}{n_0(x_{sp})}\frac{L_{n_e}}{\rho_s}\nu^{\frac{1}{3}} \longrightarrow n_e,$$

8

$$\frac{\tilde{T}_e}{T_e(x_{sp})}\frac{L_{T_e}}{\rho_s}\nu^{\frac{1}{3}} \longrightarrow T_e,$$

$$\frac{e\tilde{\phi}}{T_e(x_{sp})}\frac{L_{t_e}}{\rho_s}\frac{\nu^{\frac{1}{3}}}{\Lambda} \longrightarrow \phi.$$

Here, $\tau_0^{-1} = \Lambda\Omega_{*0}\nu^{\frac{1}{3}}$, and $L_0 = \rho_s\nu^{-\frac{1}{3}}$, where $\Omega_{*0} = \frac{c_{se}}{L_{T_e}}, \nu = \frac{2\sqrt{1+\tau}L_{T_e}}{\Lambda L_x}$, $\tau = \frac{T_e}{T_i}$, $\delta =$

$\frac{T_i}{\Lambda T_e}\frac{L_{T_e}}{L_n}(1+\eta_i)$, and $c_{se} = \sqrt{\frac{T_e(x_{sp})}{m_i}}$. With these normalizations, the intrinsic anomalous

cross-field diffusivity is normalized to χ_0 evaluated at the separatrix, where

$$\chi_0 = \frac{L_0^2}{\tau_0} = \frac{c_{se}\rho_s^2\Lambda}{L_{T_e}}\left(\frac{\Lambda L_x}{2\sqrt{1+\tau}L_{T_e}}\right)^{\frac{1}{3}} \tag{7}$$

In addition to FLR stabilizing effects, dissipative processes at large k are represented by

adjustable damping terms μ and κ, which physically represent classical viscosity $\mu_i = \frac{3}{10}\rho_i^2\nu_i$

and diffusion $\kappa_e = 4.7\rho_e^2\nu_{ei}$, with ν_i denoting the ion-ion collision frequency and ν_{ei} the

electron-ion collision frequency, $\mu = \frac{\mu_i}{\nu_L\rho_s^2\nu^{-\frac{4}{3}}}$ and $\kappa = \frac{\kappa_e}{\Lambda\Omega_{0*}\nu^{-\frac{4}{3}}}$.

Since the electron and ion temperatures are decoupled [12] and the ion temperature

evolution does not seem to play a key role in the ETG-mode, a constant and finite ion

temperature is assumed as a first approximation in modeling the boundary plasma. (A

complete theory, however, must include a self-consistent evolution for T_i). Since the electron

temperature equation and the vorticity equation are decoupled from the electron density

9

equation:

$$\frac{\partial}{\partial t}n_e - \nabla \cdot [n_e \nabla_\perp \phi \times z] = -\frac{\partial \phi}{\partial y} + D_\nu \nabla_\perp^2 n_e + \begin{cases} C_n(n_e + \frac{Ln_e}{2LT_e}T_e) & x > x_{sp} \\ \\ 0 & x < x_{sp}, \end{cases}$$

where $C_n = \nu^{\frac{2}{3}}(1 - \eta_r)$ with recycling coefficient $\eta_r = 0.96$, and D_ν is a adjustable high-k damping term, the electron density evolution equation is included as diagnostics to give the particle flux driven passively by the turbulence. As discussed in Ref. [10], to leading order in powers of $\frac{1}{\Lambda}$ in the energy end-losses, the system of equations (6) resembles the two-field-drift wave model of Hasegawa and Wakatani([14], [15], [16]). However, the higher order in $\frac{1}{\Lambda}$ is necessary in order to keep the electron-energy end-loss damping effect in the long-wavelength limit.

3.1 Linear Analysis

The linear characteristics of the instability are well understood and there have been some extensions to electromagnetic regimes, finite-$k_\parallel$ effects, and linear penetration to the edge across the separatrix ([10], [17]). However, in most of these previous analyses the efforts were focused on the fastest growing modes and mixing-length estimates for the transport, and the electron energy end-loss damping term was thought to be small and negligible. Such considerations result in a broad spectrum of instability and cannot be used in simulations unless the large (arbitrary) adjustable damping terms are used for large k and the box size

is used as a long-wavelength cut-off for the instability. Using nonvanishing electron energy end-loss terms (C_ϕ, C_T), and linearizing Eq. (6) — assuming an explicit time dependence $exp(-i\omega t)$ — yield the following normalized dispersion relation:

$$\hat{\Omega}^2 \hat{k}_\perp^2 + \hat{\Omega}\left[\hat{k}_y \hat{k}_\perp^2 \delta + i(1 + \hat{C}_T \hat{k}_\perp^2)\right] + \left[(\hat{C}_\phi - \hat{C}_T) - i\hat{k}_y(1 - \delta\hat{k}_\perp^2 \hat{C}_T)\right] = 0 \qquad (8)$$

where $\hat{\Omega} = \frac{\omega \nu^{-\frac{1}{3}}}{\Lambda\Omega_{*0}}$, and $\hat{k}_{y,\perp} = k_{y,\perp}\nu^{-\frac{1}{3}}$. Fig. 2 shows the growth rate and frequency (without high-k damping). The growth rate of the unstable mode reaches a peak value at $\hat{k}_y = 1.8$ and $\hat{k}_x = 0$ with a long-wavelength cut-off due to the electron energy endloss and a short-wavelength cut-off due to the ion-diamagnetic drift and electron energy endloss. With the high-k damping $\mu = 0.0025$ and $\nu = 0.0025$ used in this paper, it has been found almost no change over the entire growth-rate spectrum. For DIII-D parameters, $T_e(s_d) = 25\text{eV}, \tau = 0.5, \Lambda = 3.2, L_{T_e} = 1.5\text{cm}$, and $L_z = 20\text{m}$, the maximum growth rate and the corresponding frequency are $\gamma_{max} = 0.38\Lambda\Omega_{*0}\nu^{\frac{1}{3}} \sim 3.46\times 10^5 sec^{-1}, \omega_{max} = 0.52\Lambda\Omega_{*0}\nu^{\frac{1}{3}} \sim 4.74\times 10^5 sec^{-1}$, and $(k_y\rho_s)_{max} = 1.8\nu^{\frac{1}{3}} \sim 0.16$. Thus, the mode is robustly unstable for $k_\perp\rho_s \simeq 0.1$.

3.2   2d Fluid Code

A numerical code has been developed to solve the nonlinear coupled equations in (6) on a 2d grid. Spatial derivatives are evaluated to second-order accuracy in grid spacing Δ. A Fourier transform in y and a tridiagonal matrix algorithm in x (due to the non-periodic
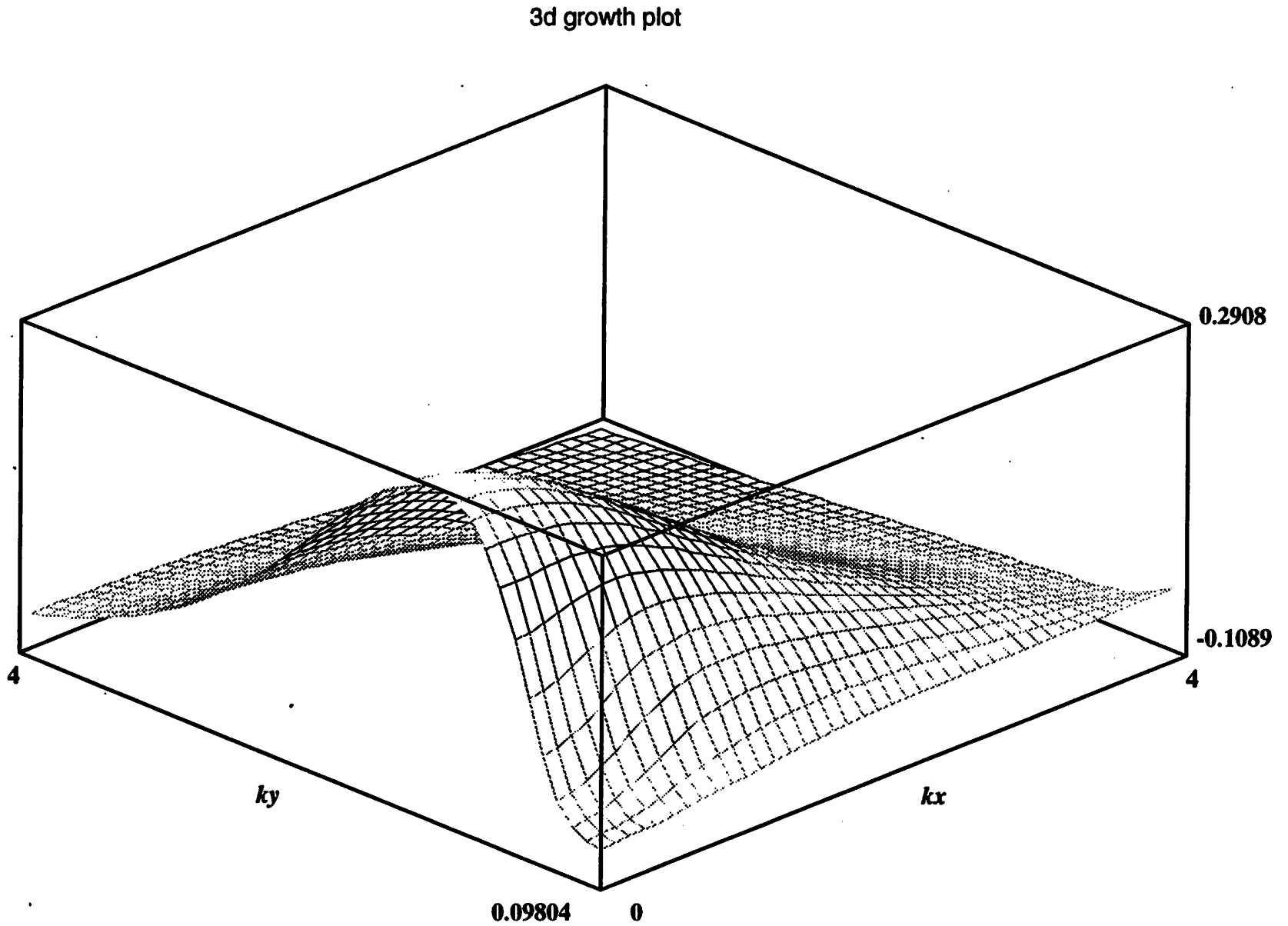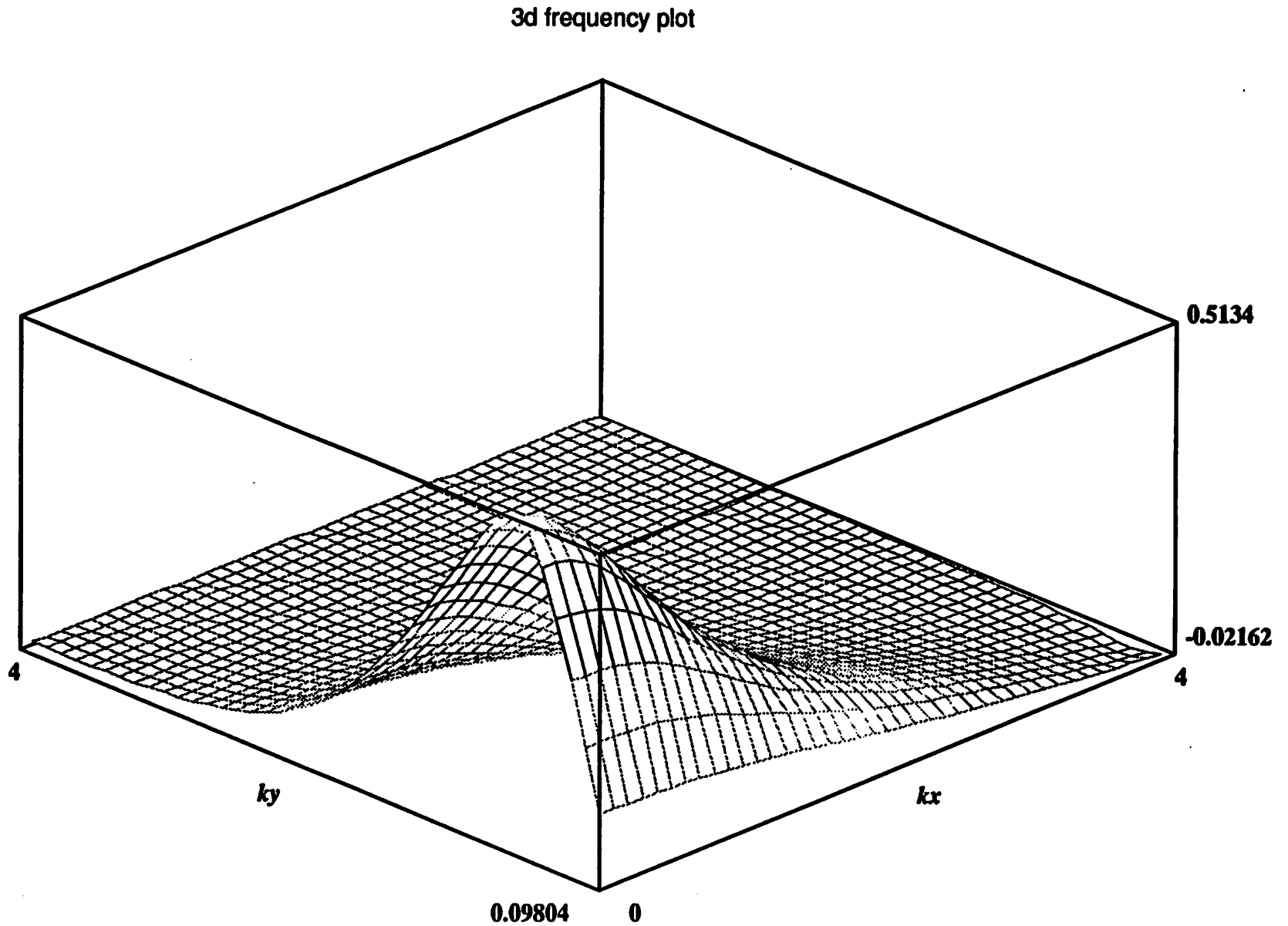
Figure 2(a): 3d plots of linear dispersion relation in Eq. (8) for the ETG-mode without a magnetic separatrix and the edge plasma region for $\tau = 1.0$, $\Lambda = 3.2$, $L_{T_e} = L_{n_e} = L_{T_i} = 1.5$ cm and $L_z = 20$ m. (a) Growth rate $Im\,(\hat{\Omega})$ vs. $\hat{k}_x$ and $\hat{k}_y$.

3d frequency plot

0.5134

-0.02162

4

4

ky

kx

0.09804   0

Figure 2(b):   3d plots of linear dispersion relation in Eq. (8) fo rthe ETG-mode without a magnetic separatrix and the edge plasma region for $\tau = 1.0$, $\Lambda = 3.2$, $L_{T_e} = L_{n_e} = L_{T_i} = 1.5$ cm and $L_z = 20$ m. (b) Frequency Re(Ω) vs. $\hat{k}_x$ and $\hat{k}_y$.

nature in radial direction x) are used to invert the vorticity $\nabla_\perp^2 \phi(x, y)$ to give $\phi(x, y)$. Time stepping is carried out using an explicit second-order Runge-Kutta scheme. The boundary conditions applied to T_e, ϕ and n_e in the y direction are periodic. The boundary conditions in the x direction are $\tilde{T} = \tilde{\phi} = 0$ at $x = 0$ and $x = L_x$. Simulation parameters are for DIII-D $L_{T_e} = L_{n_e} = L_{T_i} = 1.5\text{cm}, \tau = 1, L_z = 20\text{m}, L_x = 3\text{cm}, L_y = 39.328\text{cm}, N_{gx} = 32, N_{gy} = 256$, and $\mu = \nu = D_\nu = 0.0025$ (these are reasonable values if the neoclassical factor $(1 + 0.7q_a^2)$ in Pfirsch-Schluter regime is taken into account in front of κ_e and μ_i). Here, the choice of L_z corresponds to the connection length for a double null divertor configuration near the separatrix and L_y is chosen to put the fastest growing mode in the 10th mode-number in the simulations. Careful tests have been completed over the entire range of parameters surveyed to verify that the results are not grid-sensitive. The simulation results show that the observed linear instability agrees well with theory and the doubly periodic (x and y) version of the code has been benchmarked with a pseudospectral code showing good agreement.[18]

4   Numerical Simulation Results

This section presents the results of the nonlinear non-self-consistent fluid simulations. In order to study the basic nonlinear physics, the general trends of the ∇T_e-driven turbulence

for a given electron-temperature profile are discussed. An inverse cascade of mode energy is discussed first. The mode penetration across the separatrix into the edge region is followed. The transport measurements are presented next, and the conclusions of simulations will given last.

4.1 Energy Transfer dynamics of ∇T_e-driven modes

In Eq. (6), the mode-coupling processes are mediated by two nonlinearities, due to polarization drift and $\mathbf{E} \times \mathbf{B}$ drift respectively. Spectral transfer and its characterization in terms of cascades by the nonlinearities have long been a central part of the conceptualization of turbulence. The most widely used method of determining cascade directions is based on equilibrium statistical mechanics ([19], [20]). It has been conjectured that the $\mathbf{E} \times \mathbf{B}$ drift nonlinearity alone tends to transfer energy to small scales ([21], [22]), while the polarization-drift nonlinearity alone transfers energy to large scales [23]. From simple estimates of the two nonlinearities, it has been found that the polarization drift nonlinearity dominates the $\mathbf{E} \times \mathbf{B}$ drift nonlinearity, that is,

$$\frac{\nabla \cdot [\nabla_\perp^2 \phi \nabla_\perp \phi \times z]}{\nabla \cdot [T_e \nabla_\perp \phi \times z]} \sim \frac{\hat{k}_{\perp,m}^2 \hat{\omega}_m}{\hat{k}_{ym}} > 1,$$

where subscript m denotes that the corresponding quantities take the values at the maximum growth rate $Im(\hat{\Omega})$. Thus an inverse cascade of energy to long wavelengths is expected.

13

Fig. 3 shows a contour plot of $|\phi(m, t, x_{sp})|^2$ in the $m - t$ plane at the separatrix. Since initially all poloidal mode numbers m in y-direction ($k_y = \frac{2\pi m}{L_y}$) are set to have equal values of the mode amplitudes, the most unstable mode dominates over others around $m = 10$ as time evolves. After several linear instability cycles, nonlinear terms start to play a role; a dual-cascade of mode energy subsequently occurs, but most of the mode energy transfers to low-m modes. At steady state, the turbulence is driven around the ($m = 10$)-mode by the ∇T_e instability, damped at short-wavelengths by FLR effects as well as classical viscosity and diffusion, and transfered to long-wavelengths. This results in a stationary spectrum that is peak at low-m, as shown in Fig. 4.

4.2 Penetration across the separatrix into the edge region of the ∇T_e-driven mode

The ∇T_e-mode is an endloss-driven instability in the scrape-off layer. The penetration of the fluctuations across the separatrix into the edge is an important issue. The linear analysis of the problem has been considered by Xu, Rosenbluth, and Diamond [17]. The results have shown that the fluctuations decay exponentially on the scale of the poloidal wavelength k_y^{-1} inside the magnetic separatrix in the magnetic shearless case, and the magnetic shear limits the penetration of the potential fluctuation. These basic phenomena have been observed in linear simulations. In Fig. 4, it is apparent that the fluctuations propagate inside the
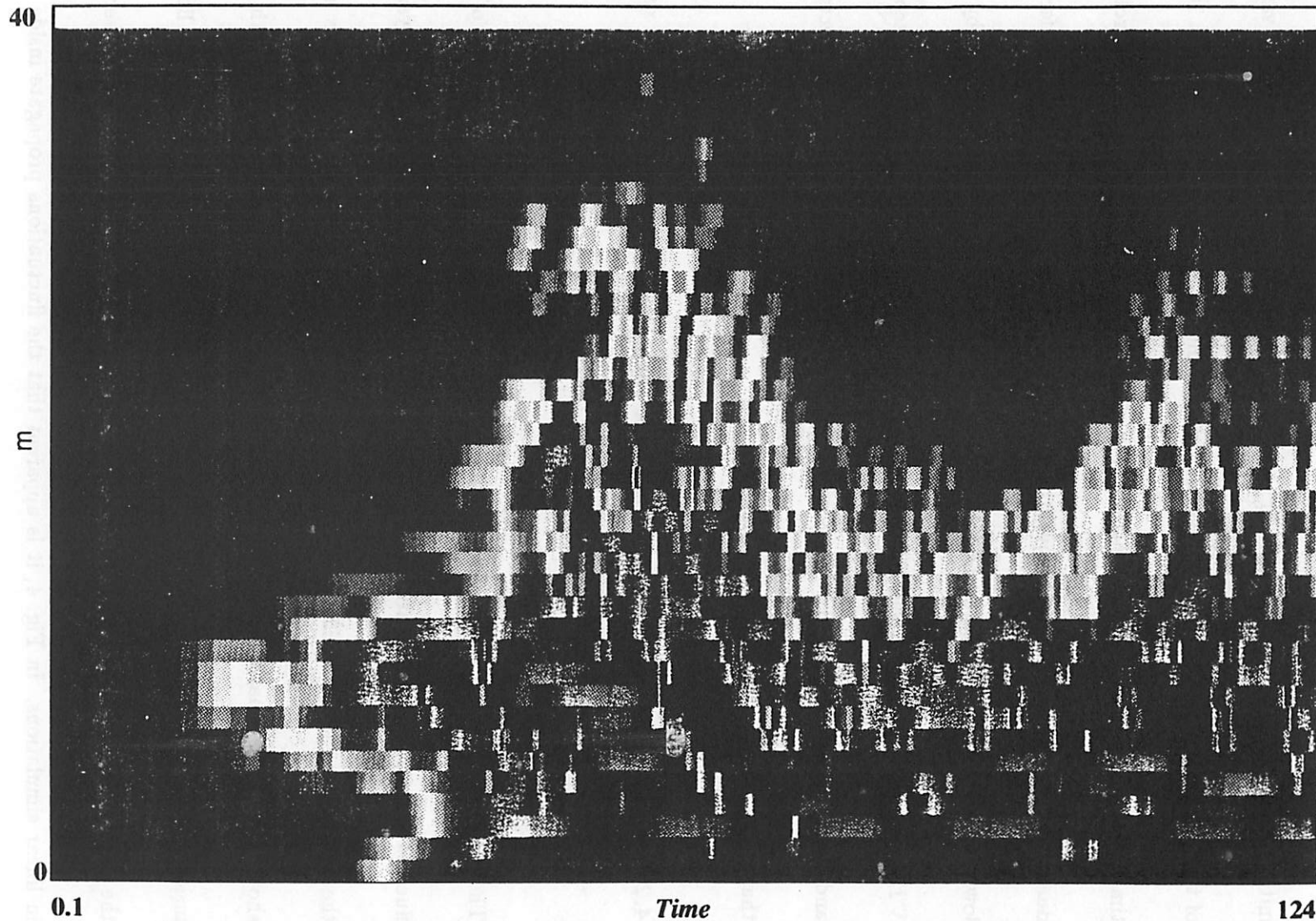
$$|\Phi(m,t,x_{sp})|^{2}$$

Figure 3: 2d contour plot of $|\phi(m,t,x=x_{sp})|^{2}$ for $x_{sp}=1.5$ cm in the SOL region, where m denotes the poloidal mode number in the y-direction ($k_{y}=\frac{2\pi m}{L_{y}}$), time t is normalized as in the text. The color code corresponds to the light spectrum. The purple represents the highest intensity, and the red the lowest intensity.
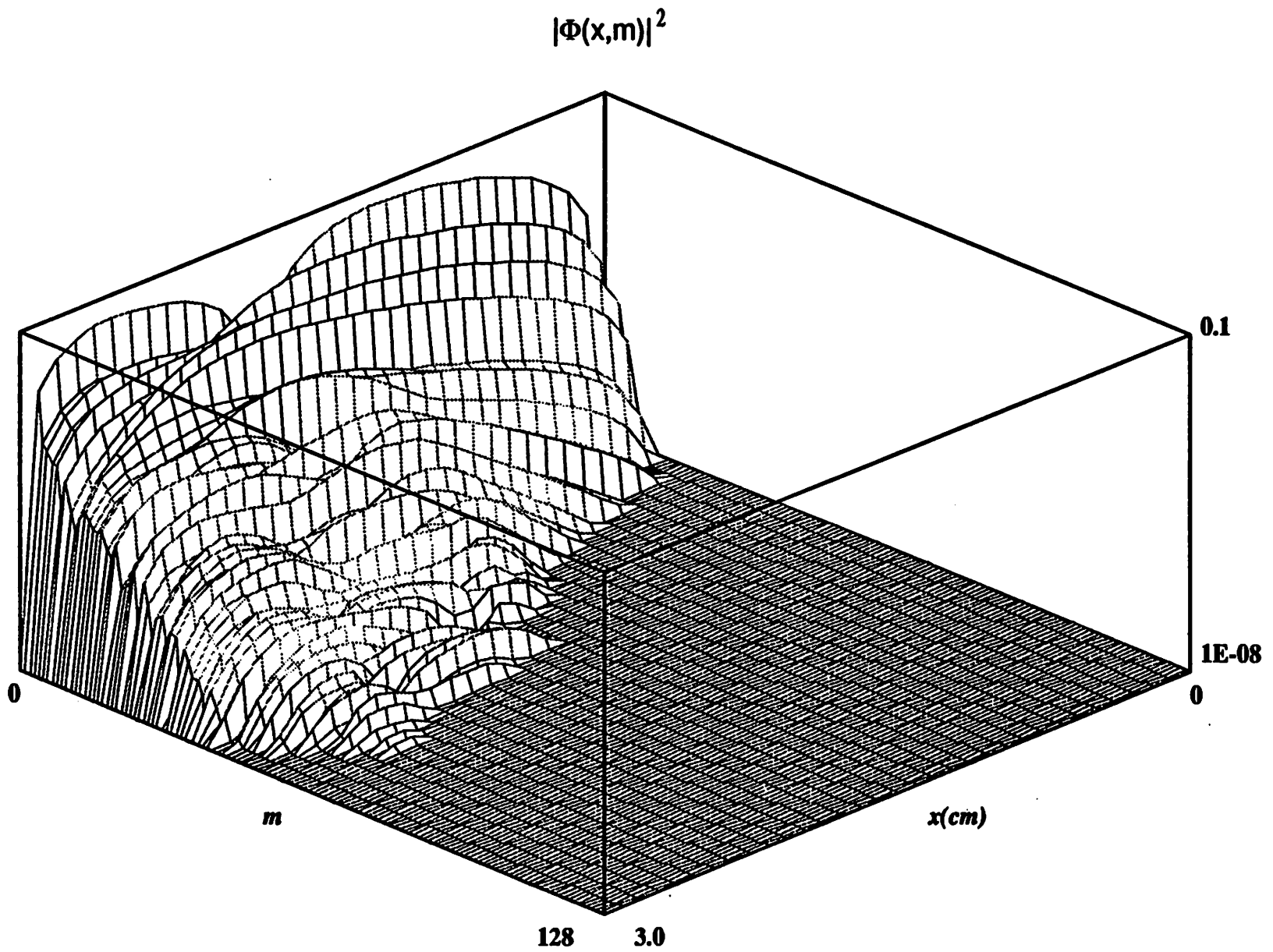
Figure 4: A snapshot of the power spectrum $|\phi(x,m)|^2$. A separatrix is located at $x = 1.5$ cm.

separatrix, and peak primarily near the separatrix. It is interesting to note from Fig. 4 that low-m fluctuations have stronger penetration than high-m fluctuations, as is expected from linear calculations with $\phi(x, k_y) \sim \exp(-k_y x + i k_y y)$ [17].

4.3 Transport measurements

In order to obtain transport estimates from the nonlinear terms, we average the electron temperature equation over y yielding

$$\frac{\partial}{\partial t} < T_e > + \frac{\partial}{\partial x} < v_x T_e > = \begin{cases} C_\phi < \phi > - C_T < T_e > & x > x_{sp} \\ \\ 0 & x < x_{sp}. \end{cases}$$

The turbulence-induced heat transport in the radial direction x arising from the $\mathbf{E} \times \mathbf{B}$ dynamics is

$$Q_x(x) = < v_x T_e > = -\chi_e \frac{\partial < T_e >}{\partial x} \tag{9}$$

where the last relation defines an effective thermal diffusivity, χ_e. The time-averaged profile of χ_e is shown in Fig. 5. The χ_e profile peaks at the separatrix and falls to zero at the simulation boundaries. The simulation results are also compared with conventional mixing-length estimates of transport:[10]

$$\chi_e^{ml} \simeq \gamma_m / \hat{k}_m^2, \tag{10}$$

where $\hat{k}_m$ is the wavelength at the maximum growth rate γ_m. For the simulation parameters with $\delta = 0.6$, it has been found $\frac{\chi_e^{ml}}{\chi_e^{sim}} \simeq 5$.
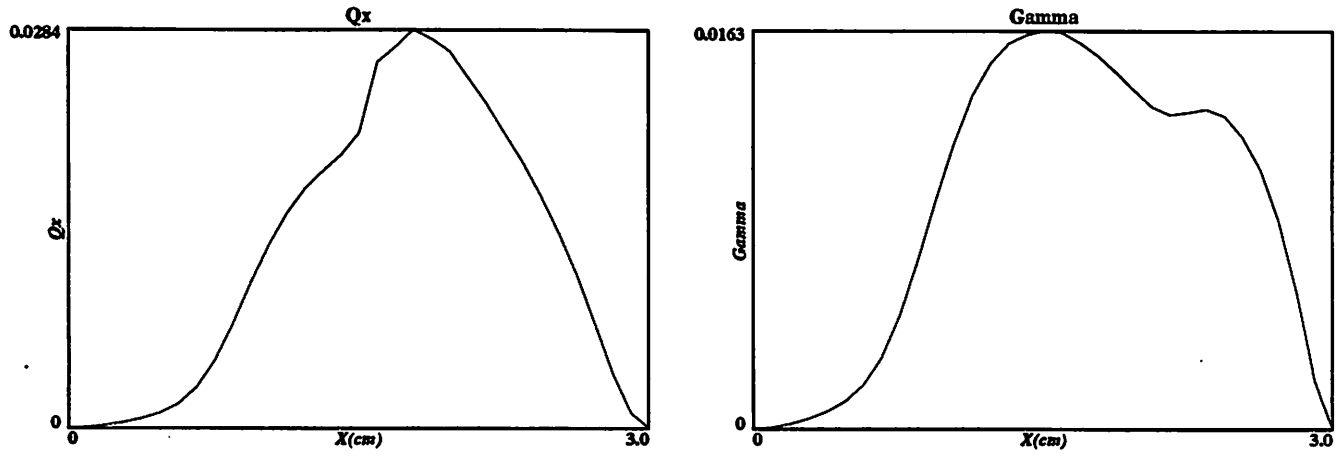
15

Turbulence Fluxes
Delta=0.6

Figure 5:   The time averaged radial profiles for the normalized turbulence heat flux $Q_x(x)$ and the particle flux $\Gamma_x(x)$. a separatrix is located at $x = 1.5$ cm.

4.4 Conclusions of Simulations

The time-averaged profiles of the fluctuation potential $\phi(x) = <\phi(x,y,t)>_{t,y}$, the electron temperature $T_e(x) = <T_e(x,y,t)>_{t,y}$, the density $n_e(x) = <n_e(x,y,t)>_{t,y}$ and the vorticity $\omega(x) = <\nabla^2_\perp \phi(x,y,t)>_{t,y}$ are shown in Fig. 6. The fluctuation profiles peak near the separatrix and fall to zero at the boundaries. The fluctuation level scalings can be estimated by the peak value near the separatrix, yielding

$$\frac{e\tilde{\phi}}{T_e(x_{sp})} \sim 0.325 \frac{\rho_s}{L_{T_e}} \Lambda \left(\frac{\Lambda L_z}{2\sqrt{1+\tau}L_{T_e}}\right)^{-\frac{1}{3}},$$

$$\frac{\tilde{T}_e}{T_e(x_{sp})} \sim 0.67 \frac{\rho_s}{L_{T_e}} \left(\frac{\Lambda L_z}{2\sqrt{1+\tau}L_{T_e}}\right)^{-\frac{1}{3}},$$

$$\frac{\tilde{n}_e}{n_0(x_{sp})} \sim 0.8 \frac{\rho_s}{L_{T_e}} \left(\frac{\Lambda L_z}{2\sqrt{1+\tau}L_{T_e}}\right)^{-\frac{1}{3}}.$$

The general formula for the time-averaged profiles of anomalous transport χ_e and D_e is $(\chi_e)^{sim}_{an} \sim f_1(\delta)f_2(x)f_3(\nu^{\frac{2}{3}})\chi_0$, the peak values near the separatrix are

$$(\chi_e)^{sim}_{an} \sim 0.0284 \frac{3c_{se}\rho_s^2\Lambda}{2L_{T_e}} \left(\frac{\Lambda L_z}{2\sqrt{1+\tau}L_{T_e}}\right)^{\frac{1}{3}}, \tag{11}$$

$$(D_e)^{sim}_{an} \sim 0.0163 \frac{c_{se}\rho_s^2\Lambda}{L_n} \left(\frac{\Lambda L_z}{2\sqrt{1+\tau}L_{T_e}}\right)^{\frac{1}{3}}, \tag{12}$$

For typical DIII-D SOL parameters: $T_e(s_d) = 25eV, \tau = 1.0, \Lambda = 3.2, L_{T_e} = 1.5cm$ and $L_z = 20m$, the predicted fluctuations are $\frac{e\tilde{\phi}}{T_e(x_{sp})} \sim 55.09\%$, $\frac{\tilde{T}_e}{T_e(x_{sp})} \sim 12.43\%$, $\frac{\tilde{n}_e}{n_0(x_{sp})} \sim 14.84\%$, $\chi^{sim}_{an} \sim 0.3m^2sec^{-1}, D^{sim}_{ean} \sim 0.115m^2sec^{-1}$, and the ratio of electron thermal diffu-sivity to the particle diffusion coefficient is $\frac{\chi^{sim}_{an}}{D^{sim}_{ean}} \sim 2.6$, which is reasonably close to recent

16

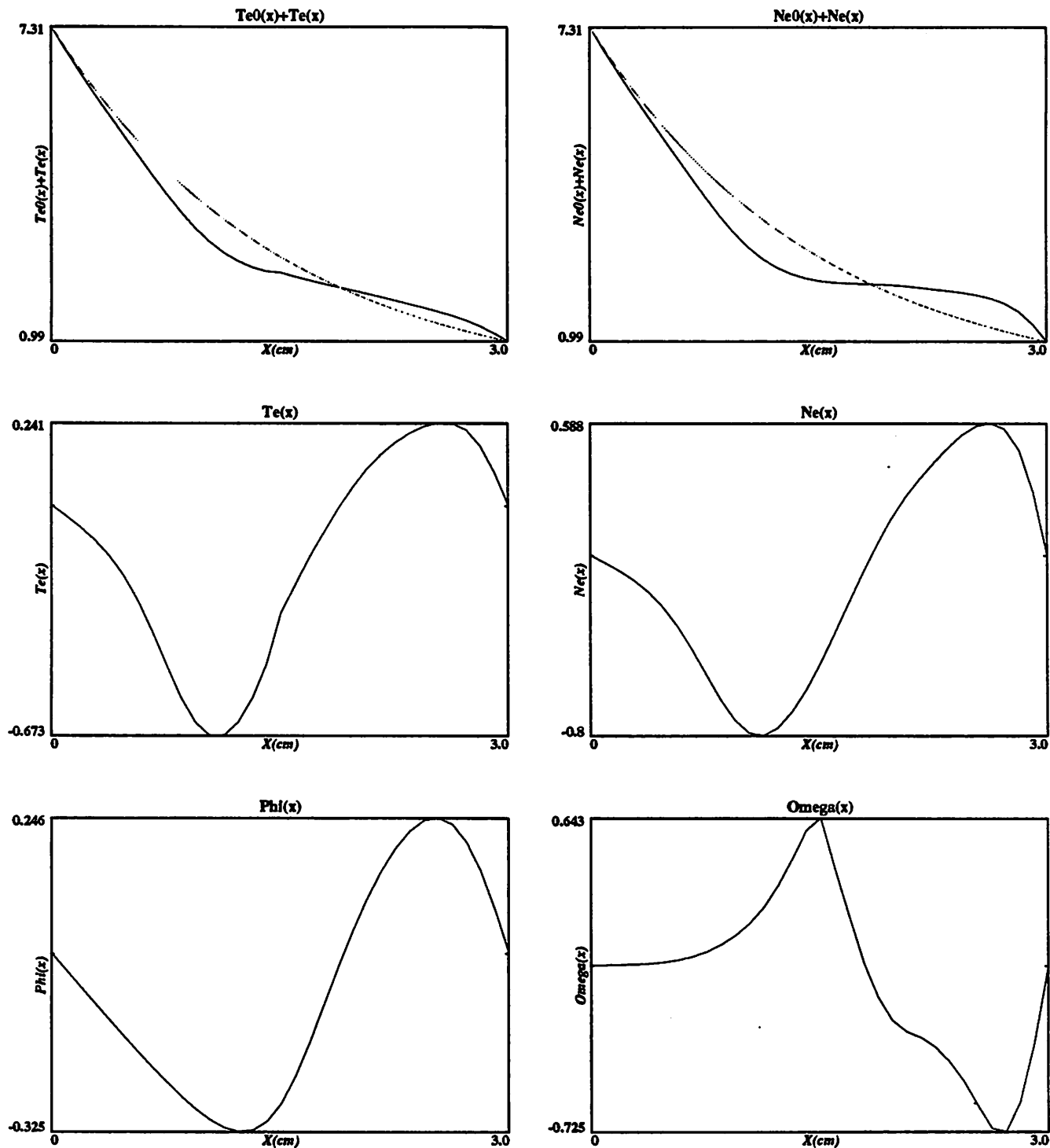# Time Averaged Radial Profiles
Delta=0.6

Figure 6: The time averaged radial profiles for the normalized total temperature $T_0(x) + T_e(x)$ and density $n_0(x) + n_e(x)$, the perturbed temperature $T_e(x)$ and the density $n_e(x)$, the potential $\phi(x)$ and the vorticity $\omega(x)$. A separatriex is located at $x = 1.5$ cm.

experimental results $\frac{\chi_{an}^{sim}}{D_{an}^{sim}} \sim 3 - 7$. From the mixing-length theory, it has been estimated that the absolute fluctuation level is $\tilde{T}_e/T_e \simeq 1/k_y L_T e \simeq 10\%$.[10] Thus there is a tendency for large fluctuation amplitudes and yet small transport. The spectrum plot (Fig. 4) and the average radial profiles (Fig. 6) would suggest that the fluctuation quantities try to take the longest radial wavelength in the simulation system, indicatiing that a small-step cross field diffusion model is inadequate. Instead, the equilibrium profile is possibly set up by relaxation to a state of minimum equilibrium enstrophy.[13]

5 Self-Consistent Simulations of $T_e(x)$ Profile in the SOL

The nominal analysis of the SOL assumes that the power entering the SOL is equal to that crossing the separatrix. An estimate of the $T_e(x)$ profile can be made by balancing the anomalous radial and classical axial electron power flows in the SOL electron-conduction layer. The uncertainty in the analysis is due to the uncertainty in the nature of the SOL turbulence and its related anomalous transport. This section presents self-consistent simulations in order to give the electron temperature profile in the SOL due to ∇T_e-driven turbulence. The radial simulation domain is divided into three regions: the edge region, the source region and the SOL. In the source region, the plasma is heated by an external source term H representing either the heating or power generated in the core plasma. The

normalized fluid equations in our simulations are

$$\frac{\partial}{\partial t}\nabla_\perp^2\phi + \{\phi, \nabla_\perp^2\phi\} = \delta e^{-\frac{x-x_{sp}}{L_{T_i}}}\frac{\partial}{\partial y}\nabla_\perp^2\phi + \mu\nabla_\perp^4\phi + \begin{cases} \hat{J}_\parallel, & x > x_{sp} \\[2ex] 0, & x < x_{sp} \end{cases}$$

$$\frac{\partial}{\partial t}T_e + \{\phi, T_e\} = -e^{-\frac{x-x_{sp}}{L_{T_e}}}\frac{\partial\phi}{\partial y} + \kappa\nabla_\perp^2 T_e + \begin{cases} \hat{q}_\parallel, & x > x_{sp} + \Delta_H \\[2ex] \hat{q}_\parallel + H, & x_{sp} < x < x_{sp} + \Delta_H \\[2ex] 0, & x < x_{sp} \end{cases} \quad (13)$$

where

$$\hat{J}_\parallel = \frac{L_{T_e}\nu^{\frac{1}{3}}}{\Lambda\rho_s}\left(\frac{\hat{c}_s}{K_i} - \frac{\hat{v}_{T_e}}{2\sqrt{\pi}}\right)$$

$$\hat{q}_\parallel = \nu^{\frac{2}{3}}\hat{v}_{T_e}\left\{2\left(T_e + \frac{L_{T_e}\nu^{\frac{1}{3}}}{\rho_s}e^{-\frac{x-x_{sp}}{L_{T_e}}}\right) + \left(\Lambda\phi + (\Lambda+\hat{\Lambda})\frac{L_{T_e}\nu^{\frac{1}{3}}}{\rho_s}e^{-\frac{x-x_{sp}}{L_{T_e}}}\right)\right\}$$

$$\hat{v}_{T_e} = \sqrt{\frac{2m_i\left(e^{-\frac{x-x_{sp}}{L_{T_e}}} + T_e\frac{\rho_s}{L_{T_e}\nu^{\frac{1}{3}}}\right)}{m_e(1+1/\tau)}}\ \exp\left(-\frac{(\Lambda+\hat{\Lambda})e^{-\frac{x-x_{sp}}{L_{T_e}}} + \Lambda\phi\frac{\rho_s}{L_{T_e}\nu^{\frac{1}{3}}}}{e^{-\frac{x-x_{sp}}{L_{T_e}}} + T_e\frac{\rho_s}{L_{T_e}\nu^{\frac{1}{3}}}}\right),$$

$$\hat{c}_s = \sqrt{\frac{e^{-\frac{x-x_{sp}}{L_{T_i}}}/\tau + e^{-\frac{x-x_{sp}}{L_{T_e}}} + \frac{T_e\rho_s}{L_{T_e}\nu^{\frac{1}{3}}}}{1+1/\tau}},$$

$$\hat{\Lambda} = \ln\left(\sqrt{\frac{e^{-\frac{x-x_{sp}}{L_{T_e}}} + T_e\frac{\rho_s}{L_{T_e}\nu^{\frac{1}{3}}}}{\hat{c}_s^2}}\right),$$

Here L_{T_e} and L_{T_i} represent the initial electron and ion temperature gradients. The very

steep electron temperaure profile is chosen representing neoclassical cross-field transports

with $L_{T_e} = 5$mm. Since the electron and ion temperatures are decoupled in the SOL, and the

ion temperature has a larger radial scale length than the electron temperature (as suggested

by the DIII-D SOL data[24]), for simplicity, a flat ion temperature profile is chosen. The

relation of the normalized source term H with the power crossing the separatrix P_e is given

by

$$H = \left(\frac{L_{T_e}}{\rho_s}\right)^2 \frac{P_e}{\Lambda L_z L_y n_e c_s T_e(x_{sp})} \frac{\rho_s}{\Delta_H} \tag{14}$$

The simulation parameters are $T_e(x_{sp}) = 100\text{eV}, L_z = 20\text{m}, L_y = 39.328\text{cm}, L_x = 5.0\text{cm}, \Delta_H = \frac{3}{8}L_x$, and $\Lambda = 3.2$. For $n_e = 2 \times 10^{13}\text{cm}^{-3}, P_e = 1\text{MW}$, and $H = 0.0084$. For the given

power $P_e = 2\text{MW}$, the electron temperature profile from self-consistent simulations are

shown in Fig. 7. The dotted curve represents the initial profile and the broken line is the

profile produced by the neoclassical diffusion (or numerical diffusion with $\mu = \kappa = 0.0025$)

by taking $\tau = 0.125$ (in this case, the ETG-mode is completely suppressed by the FLR

effects). The solid curve is the profile produced by anomalous transport in the presence

of the ETG-mode by taking $\tau = 0.5$. All of these electron temperature profiles appear

to fall off exponentially in the radial (x) direction, but the ETG-mode driven turbulence

broadens the profiles dramatically with $L_{T_e} \simeq 1.0\text{cm}$, which is consistent with experimental
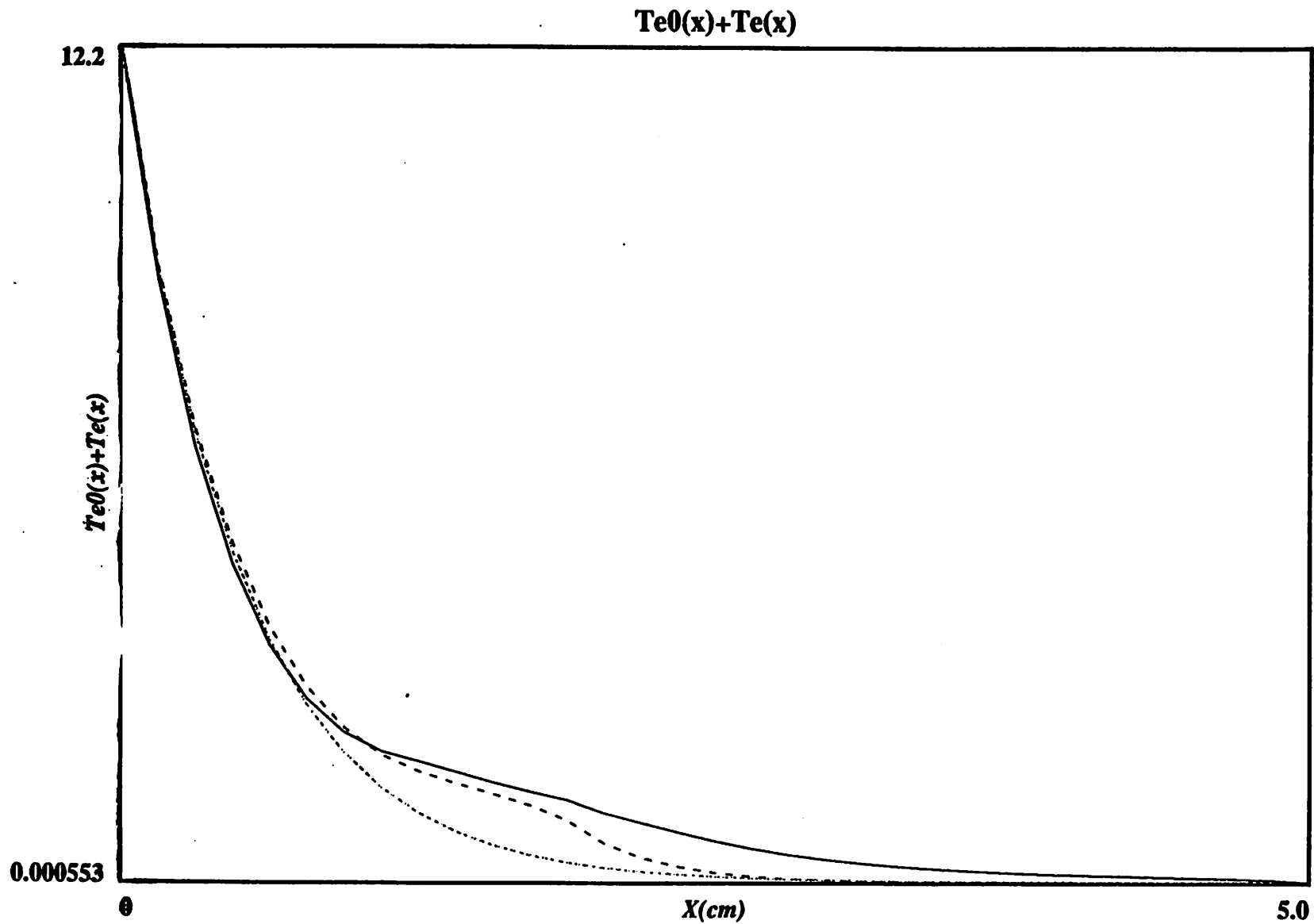
measurements of the $L_{T_e} \sim 0.5$ to 1cm.[25]

Te0(x)+Te(x)

Figure 7(a):   Time averaged radial profiles for the normalized temperature $T_0(x) + T_e(x)$ in the boundary plasmas (a).
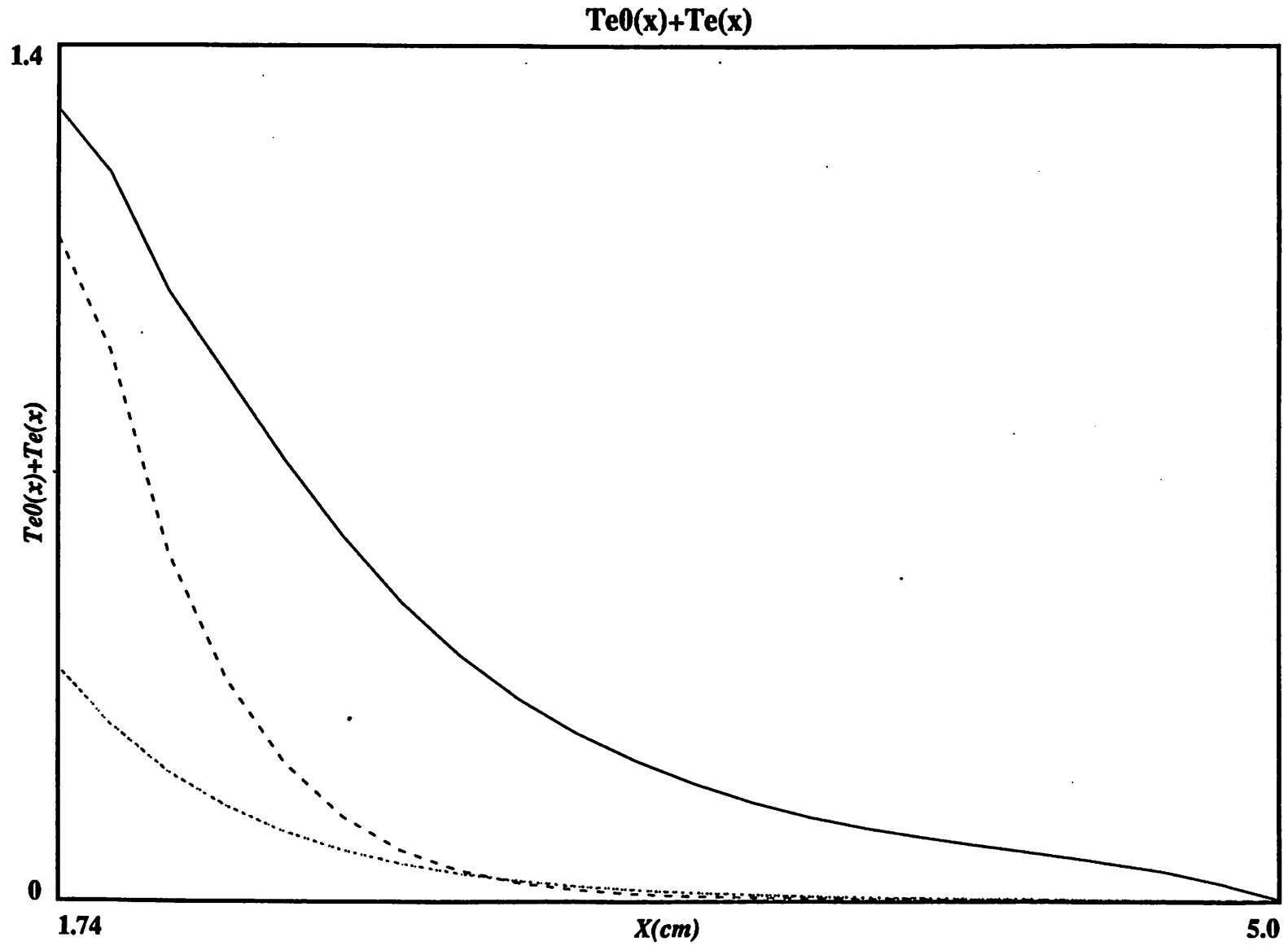
Te0(x)+Te(x)

Figure 7(b): Time averaged radial profiles for the normalized temperature $T_0(x) + T_e(x)$ in the SOL (b).

6 Conclusions

This paper represents the first step in the 2d nonlinear fluid simulations of the electron temperature gradient driven turbulence in the tokamak boundary plasmas. It has been found that the mode energy inversely cascades to long wavelengths because of the polarization drift nonlinearity, and thus connects to the radial scale of the equilibrium. The instability driven in the SOL is strongly peaked at the LCFS and penetrates into the edge plasma significantly in the long-wavelength limit. In the absence of a heat source from the core plasma, as the results in Section 4, the nonlinear saturation of the instability is due to quasilinear flattening. The associated heat flux is much larger than the neoclassical one but is a factor five of smaller than a mixing-length estimates, and the large-scale radial structures of fluctuation quantites indicate that the cross-field transport is not diffusive.

The SOL profile is set by the balance of the anomalous radial heat transport with axial loss to the divertor (limiter) plates. In order to obtain a SOL electron temperature profile, a source term is included in the simulations as in experiments. Fig. 8 shows that the electron temperature falls off exponentially with the width around 1cm. Most importantly FLR (parametrized by $\tau = T_e/T_i$) effects have been found to strongly stabilize the mode and therefore suppress the turbulence. As the power crossing the separatrix is increased from $P_e = 1\text{MW}$ to $P_e = 2\text{MW}$ and to $P_e = 3\text{MW}$, it has been observed that the electron

temperature at the separatrix rises, but the exponential profile and the SOL width show almost no changes, which is consistent with the experimental observations[25].

The simulation results concerning the ∇T_e-driven turbulence in the tokamak boundary plasmas have important experimental implications. Since the level of transport and the SOL width observed here are experimently quite reasonable, it suggests the ∇T_e-driven turbulence as a possible mechanism for explaining the exponential profiles in the SOL electron conduction layer. With neoclassical perpendicular transport in the SOL, the power crossing the separatrix would be rapidly lost to the endplates along the magnetic field line, giving a narrow temperature gradient near the separatrix ($L_{T_e} \sim 5mm$). The ∇T_e-driven turbulence would then be driven strongly unstable and an outward heat flux would ensue, until a balance between the perpendicular $E \times B$ transport due to the ETG-mode and parallel losses to the plates are reached. If the ∇T_e-driven mode is indeed an important constituent of the tokamak SOL turbulence, then the SOL fluctuations should exhibit a clear sensitivity to the sheath boundary conditions ($\Lambda = \frac{e\Phi_0}{T_e}$). The sheath parameter Λ can be changed experimentally by varying the materials of the limiter (or divertor) plates (and therefore their conductivity) or pumping neutral gases into the sheath regions such as in the proposed gas target divertor configurations (comparison of the collisional sheath model with experimental measurements is given in Ref. [26]) to check the the ∇T_e-driven mode.

On the other hand, since a narrow sheath region (sheath + presheath) near the endplates, with large equilibrium gradients along z (on the order of Debye length), plays a crucial role for the instability, it is desirable to resolve the sheath boundary conditions carefully by the code-merging techniques as described in Ref. [27] (merging PIC-codes in the sheath and fluid codes in the bulk).

However, the major drawback of these simulations for a comprehensive boundary plasma model is an absence of an instability drive in the edge region. Experimental evidence shows that a shear layer occurs inside the last closed flux surface, which is significant to L-H transitions. The source of this sheared flow is debatable. Three distinct mechanisms have been proposed to drive poloidal rotation in the closed flux region: ion orbit losses([7], [8], [9]), Reynold stress[28] and anomalous Stringer spin-up [29]. None of these models include the SOL physics. It has been believed that a complete model for the boundary plasma should include the dominant electron physics in the SOL and the dominant ion dynamics inside the separatrix to explain the cause of sheared flow and the SOL power handling capability. In a comprehensive boundary plasma model it is also desirable to include the parallel variation of physical quantities (such as electron temperature and density variations along the magnetic field line, both in the equilibrium and perturbed states) and the magnetic shear. Several other interesting future investigations are to include neutral gases, impurities, and toroidal

effects to simulate the coupling of the ETG-driven turbulence with the ionization-driven modes, radiation condensation modes, and interchange modes. Finally, the extension of the simulation model to electromagnetic limits may yield important insights into the finite-beta effects.

Acknowledgments

References

[1] H. L. Berk, D. D. Ryutov and Yu. Tsidulko, *Phys. of Fluids* **3**, 1364 (1991).

[2] K. H. Burrel, T. N. Carlstrom, E. J. Doyle, P. Gohil, R. J. Groebner, T. Lehecka, N. C. Luhmann, Jr., H. Matsumoto, T. H. Osborne, W. A. Peebles, and R. Philipona,

Phys. Fluids **B2**, 1405 (1990).

[3] A. J. Wooton, B. A. Carreras, H. Matsumoto, K. McGuire, W. A. Peebles, Ch. P. Ritz, P. W. Terry and S. J. Zweben, *Phys. of Fluids* **2**, 2879 (1990).

[4] R. D. Stambaugh, S. M. Wolfe, R. J. Hawryluk, H. J. Harris, H. Biglari, S. C. Prager, R. J. Goldston, R. J. Fonck, T. Okhawa, B. G. Logan and E. Oktay, *Phys. of Fluids* **2**, 2941 (1990).

[5] R. A. Moyer, J. G. Watkins, K. Burrel, R. W. Conn, R. Doerner, D. Hill, R. Lehmer, M. A. Mahdavi, L. Schmitz, and G. Tynan; *Bull. Am. Phys. Soc.* **36**, 2472(1991).

[6] F. L. Hinton, M. S. Chu, *Nucl. Fusion* **25** 345 (1985); F. L. Hinton, *Nucl. Fusion* **25** 1457 (1985)

[7] S. -I. Itoh and K. Itoh, *Phys. Rev. Lett.* **60**, 2276 (1988);

[8] K. C. Shaing, E. C. Crume, Jr. , and W. A. Houlberg, *Comments Plasma Phys. and Controlled Fusion* **12** 69 (1988); K. C. Shaing, E. C. Crume, Jr. , and W. A. Houlberg, *Phys. of Fluids* **2**, 1492 (1990).

[9] R. D. Hazeltine, *Phys. of Fluids* **B 1**, 2031 (1989).

[10] H. L. Berk, R. H. Cohen, D. D. Ryutov, Yu. Tsidulko, and X. Q. Xu submitted to *Nuclear Fusion.*

[11] W. B. Kunkel and J. U. Guillory, in *Proc. 7th Conf. on Phenomena in Ionized Gases*, (Belgrade, 1965, Ed. B. Perovic and D. Tocsic) Grad Jevinska Kniga, Belgrade, Yugoslavia(1966), V. 2, 702.

[12] W. M. Nevins, accepted by *Nuclear Fusion*.

[13] N. Mattor and R. H. Cohen, submitted to *Phys. of Fluids*.

[14] A. Hasegawa and M. Wakatani, *Phys. Rev. Lett.* **50**, 682 (1993); M. Wakatani and A. Hasegawa, *Phys. of Fluids* **27**, 611 (1984).

[15] F. Y. Gang, B. D. Scott, and P. H. Diamond, *Phys. of Fluids* **1**, 1331 (1989); F. Y. Gang, B. D. Scott, and P. H. Diamond, *Phys. of Fluids* **3**, 955 (1991).

[16] A. E. Koniges, J. A. Crotinger, and P. H. Diamond, *Phys. of Fluids* **4**, 2785 (1992).

[17] X. Q. Xu, M. N. Rosenbluth, and P. H. Diamond, submitted to *Phys. of Fluids*.

[18] A. E. Koniges, J. A. Crotinger, and P. H. Diamond, *Phys. of Fluids* **4**, 2785 (1992).

[19] R. H. Kraichnan, *J. Fluid Mech.* **67**, 155(1975).

[20] S. A. Orszag, in *Fluid Dynamics*: Les Houches, edited by R. Balin and J.-L. Peube (Gordon and Breach, New York, 1973), p. 235.

[21] P. H. Diamond and H. Biglari, *Phys. Rev. Lett.* **65**, 2865 (1990);

[22] D. E. Newman, P. W. Terry, and P. H. Diamond, *Phys. of Fluids* B4, 599 (1992).

[23] A. Hasegawa, C. G. Maclennan, and Y. Kodama, *Phys. of Fluids* 22, 2122 (1979).

[24] G. D. Porter, private communication.

[25] R. A. Jong, D. N. Hill, and G. D. Porter; *Bull. Am. Phys. Soc.* 37, 1566(1992).

[26] A. H. Futch, J. W. Cuthbertson, D. A. Buchenauer, D. N. Hill, G. F. Matthews, C. Lowry, G. D. Porter, R. A. Jong; *Bull. Am. Phys. Soc.* 37, 1567(1992).

[27] A. Tarditi, Submitted to Computer Physics Communication.

[28] P. H. Diamond and Y. B. Kim, *Phys. of Fluids* B3, 1626 (1991); J. F. Drake, J. M. Finn, P. N. Guzdar, V. Shapiro, V. Shevchenko, F. Waelbroek, A. B. Hassam, C. S. Liu, and R. Sagdeev, *Phys. of Fluids* B Lett. 4, 488(1992).

[29] A. B. Hassam, T. M. Antonsen, Jr. , J. F. Drake, and C. S. Liu, *Phys. Rev. Lett.* 66, 309 (1991);